Flow velocity oscillations in a PEM fuel cell cathode channel induced by harmonic pressure perturbations

Andrei Kulikovsky[1,2]

Forschungszentrum Jülich GmbH
Theory and Computation of Energy Materials (IEK-13)
Institute of Energy and Climate Research,
D–52425 Jülich, Germany

Abstract

To measure electrochemical pressure impedance spectra, oscillating pressure gradient is applied at the PEM fuel cell channel inlet or outlet. A model for air flow velocity oscillations induced by the AC pressure gradient is developed. The Nyquist spectrum of velocity oscillations has a form of a parallel RC–circuit electric impedance. Due to viscous forces, the amplitude of oscillations decays with the frequency. Analytical solution allows one to estimate this amplitude and the characteristic frequency of damping. A dominating effect of velocity oscillations on the pressure impedance at low air flow stoichiometries is demonstrated.

Keywords: EPIS, cFRA, PEM fuel cell, modeling

1. Introduction

In recent years, electrochemical pressure impedance spectroscopy (EPIS) has attracted attention of PEM fuel cell community as a useful tool for cell testing and characterization. The idea of EPIS suggested by Niroumand et al. [1] is simple: AC pressure perturbation δp is applied at the cathode channel inlet or outlet leads to oscillations of oxygen concentration δc in the cell. Due to oxygen reduction reaction (ORR), δc induces oscillations of the cell potential δV. The ratio $\delta V/\delta c$ or $\delta V/\delta p$ is the EPIS spectrum containing information on the oxygen and water transport processes in the cell cathode [2–8].

Basically, there are two options to produce δc: either, by perturbing pressure at the channel inlet or outlet [2, 6–8], or by periodic admixing oxygen concentration to the inlet flow, keeping the pressure as constant as possible [3–5]. For the reasons discussed below, it would be natural to name the second method *electrochemical concentration impedance spectroscopy* (ECIS).

The amplitude of pressure/concentration perturbation is usually selected to get small (linear) but measurable response of δV. Much less attention has been paid to the flow velocity oscillations (FVO) induced by the AC pressure perturbation. Numerical model of ECIS [3–5] ignores FVO, though admixing oxygen induces inlet pressure perturbation on the order of 30 Pa [5]. Below, we will show that this leads to quite a significant effect of FVO on concentration/pressure impedance spectra. The works reported numerical EPIS models [6, 7] contain no information on FVO in the channel and the role of FVO remains unclear.

It should be noted that the typical pressure perturbation in EPIS experiments is on the order of several kPa [8, 9], while in ECIS experiments this perturbation does not exceed 30 Pa [5]. Pressure signal in EPIS perturbs transport of liquid water in the cell, while in ECIS this effect is seemingly small. Below, we will be focused on the effect of velocity oscillations in channel; the transport of liquid water in the cell is out of the scope of this work.

In this work, a model for oscillating flow in a tube suggested by Sexl [10] is used to rationalize the pressure–induced FVO in a PEM fuel cell cathode channel under conditions of EPIS experiment. Analytical expression for mean over the channel radius FVO amplitude shows that viscous forces damp oscillations at the frequencies above ν/R_h^2, where ν is the air kinematic viscosity and R_h is the channel radius. The maximal FVO amplitude is achieved at low frequencies; it is proportional to the channel cross section area and to the applied pressure gradient. An example of EPIS spectrum taking into account FVO is calculated. The spectrum shows dominating contribution of the FVO to pressure impedance, meaning that the primary effect of pressure oscillations on the oxygen concentration in the catalyst layer is indirect, due to variation of air flow velocity in the channel.

Email address: A.Kulikovsky@fz-juelich.de (Andrei Kulikovsky)
[1]ISE member
[2]Also at: Lomonosov Moscow State University, Research Computing Center, 119991 Moscow, Russia

2. Model and Methods

The speed of sound in air at 60°C is 365 m s^{-1}, therefore, for the channel length on the order of 1 m, propagation of sound wave takes about $\tau_s = 1/365 \simeq 2.74 \cdot 10^{-3}$ s. This time corresponds to the frequency $f_s = 1/(2\pi\tau_s) \simeq 58$ Hz, i.e., for the frequencies below $f_{\min} \simeq 10$ Hz, propagation of sound wave equilibrating pressure gradient along the channel can be considered as immediate. Thus, for the low frequencies it does not matter whether the pressure perturbation is applied at the inlet or outlet; the effect is the same. Note that for shorter channels on the order of 10 cm, $f_{\min}$ exceeds 100 Hz. Note also that here we ignore the effect of humidifier volume on pressure perturbation. This effect will be discussed below.

Oscillations of flow velocity induced by the applied pressure perturbations can be rationalized using the model developed by Sexl [10]. For simplicity we will consider channel of a circular form. Hydrogen molecular weight is much smaller than that of oxygen and to a good approximation flow velocity variation due to replacement of O_2 molecule by two H_2O molecules in the air flow can be neglected.

Let the axis z be directed along the channel of the radius R_h and the length L. As discussed above, subsonic air flow in the channel is incompressible. The laminar flow of incompressible fluid in a circular channel has a single, independent of z axial velocity component w [11]. The Navier–Stokes equation for $w(t, r)$ has the form

$$\frac{\partial w}{\partial t} - \frac{\nu}{r}\frac{\partial}{\partial r}\left(r\frac{\partial w}{\partial r}\right) = -\frac{1}{\rho}\frac{\partial p}{\partial z} \tag{1}$$

where t is time, r is the radial coordinate, ν is the air kinematic viscosity, ρ is the air density, and $\partial p/\partial z$ is the independent of z pressure gradient.

With the dimensionless variables

$$\tilde{r} = \frac{r}{R_h}, \quad \tilde{z} = \frac{z}{L}, \quad \tilde{w} = \frac{w}{\langle w^0\rangle}, \quad \tilde{p} = \frac{p}{p^{in}}, \quad \tilde{t} = \frac{t\nu}{R_h^2}, \quad \tilde{\omega} = \frac{\omega R_h^2}{\nu} \tag{2}$$

Eq.(1) takes the form

$$\frac{\partial \tilde{w}}{\partial \tilde{t}} - \frac{1}{\tilde{r}}\frac{\partial}{\partial \tilde{r}}\left(\tilde{r}\frac{\partial \tilde{w}}{\partial \tilde{r}}\right) = \phi\left|\frac{\partial \tilde{p}}{\partial \tilde{z}}\right|. \tag{3}$$

Here, i_* is the ORR volumetric exchange current density, c_h^{in} is the reference oxygen concentration, p^{in} is the static inlet pressure of the flow, $\langle w^0\rangle$ is the average over channel radius steady–state flow velocity, and

$$\phi = \frac{R_h^2 p^{in}}{\rho\nu\langle w^0\rangle L} \tag{4}$$

is the only dimensionless parameter in the problem. Eq.(3) is linear; substituting perturbations of the form

$$\begin{aligned}\tilde{w} &= \tilde{w}^0(\tilde{r}) + \tilde{w}^1(\tilde{r}, \tilde{\omega})\exp(\mathrm{i}\tilde{\omega}\tilde{t})\\ \tilde{p} &= \tilde{p}^{in}(\tilde{z}) + \tilde{p}^1(\tilde{z})\exp(\mathrm{i}\tilde{\omega}\tilde{t})\end{aligned} \tag{5}$$

and subtracting the static equation for $\tilde{w}^0$, we get equation for the perturbation amplitude $\tilde{w}^1$:

$$\frac{1}{\tilde{r}}\frac{\partial}{\partial \tilde{r}}\left(\tilde{r}\frac{\partial \tilde{w}^1}{\partial \tilde{r}}\right) = \mathrm{i}\tilde{\omega}\tilde{w}^1 - \phi\left|\frac{\partial \tilde{p}^1}{\partial \tilde{z}}\right|, \quad \left.\frac{\partial \tilde{w}^1}{\partial \tilde{r}}\right|_{\tilde{r}=0} = 0, \quad \tilde{w}^1(1) = 0 \tag{6}$$

Here, the subscripts 0 and 1 mark the static and perturbed variables, respectively, $\partial\tilde{p}^1/\partial\tilde{z}$ is the amplitude of applied pressure perturbation gradient, which can be calculated simply by dividing $\tilde{p}^1$ by the channel length $\tilde{z} = 1$. The left boundary condition for Eq.(6) means symmetry of the solution at the channel axis, and the right boundary condition is "no-slip" one. Note that due to linearity of Eq.(3), smallness of $|\partial\tilde{p}^1/\partial\tilde{z}|$ and $\tilde{w}^1$ is, in general, not required; Eq.(6) describes perturbation of an arbitrary amplitude.

3. Results and discussion

Solution to Eq.(6) is [10]:

$$\tilde{w}^1(\tilde{r}) = -\frac{\mathrm{i}\phi}{\tilde{\omega}}\left|\frac{\partial \tilde{p}^1}{\partial \tilde{z}}\right|\left(1 - \frac{J_0\left(\sqrt{-\mathrm{i}\tilde{\omega}}\,\tilde{r}\right)}{J_0\left(\sqrt{-\mathrm{i}\tilde{\omega}}\right)}\right) \tag{7}$$

where J_0 is the Bessel function.

The features of $\tilde{w}^1$ radial shape have been discussed in [10]. For EPIS of particular interest is the frequency dependence of average over the radius velocity perturbation $\langle\tilde{w}^1\rangle$

$$\langle\tilde{w}^1\rangle = \int_0^1 \tilde{w}^1(\tilde{r})\,d\tilde{r} \tag{8}$$

Calculation of integral (8) with Eq.(7) gives

$$\langle\tilde{w}^1\rangle = -\frac{\mathrm{i}\phi}{\tilde{\omega}}\left|\frac{\partial \tilde{p}^1}{\partial \tilde{z}}\right|\left(1 - \frac{I_0\left(\sqrt{\mathrm{i}\tilde{\omega}}\right)}{J_0\left(\sqrt{-\mathrm{i}\tilde{\omega}}\right)} + \frac{\pi\left(I_1\left(\sqrt{\mathrm{i}\tilde{\omega}}\right)L_0\left(\sqrt{\mathrm{i}\tilde{\omega}}\right) - I_0\left(\sqrt{\mathrm{i}\tilde{\omega}}\right)L_1\left(\sqrt{\mathrm{i}\tilde{\omega}}\right)\right)}{2J_0\left(\sqrt{-\mathrm{i}\tilde{\omega}}\right)}\right) \tag{9}$$

where I is the modified Bessel function of the first kind, and L is the modified Struve function.

The Nyquist spectrum of Eq.(9) has the form of a parallel RC–circuit electric impedance (Figure 1). Numerical calculations show that the peak of $-\operatorname{Im}\left(\langle\tilde{w}^1\rangle\right)$ (Figure 1b) is located at the characteristic frequency f_*, which is well described by

$$f_* \simeq \frac{\nu}{R_h^2}. \tag{10}$$

Figure 2 shows the frequency dependence of the modulus and phase angle of oscillations. At small frequencies of the AC signal, flow velocity oscillates in–phase with the pressure and $-\operatorname{Im}\left(\langle\tilde{w}^1\rangle\right)$ is small. However, near the

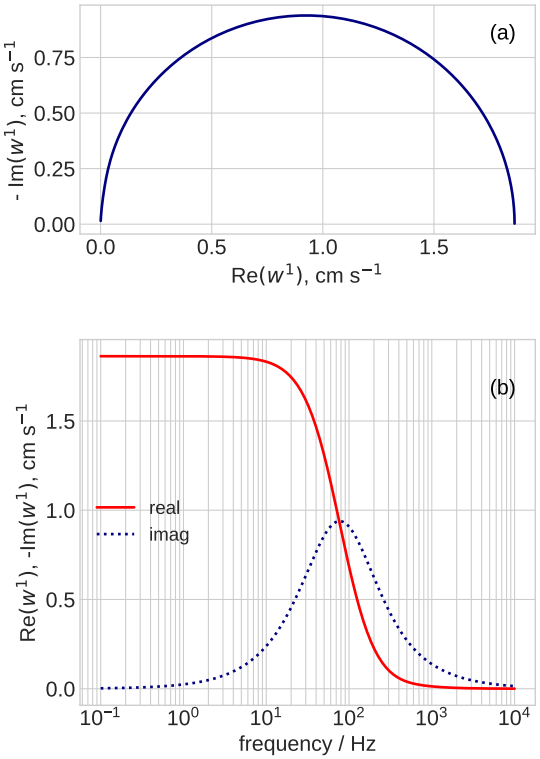

Figure 1: (a) The Nyquist spectrum of velocity pulsations in the channel, Eq.(9). (b) The frequency dependence of real and imaginary part of Eq.(9). Parameters for the calculation are listed in the upper part of Table 1.

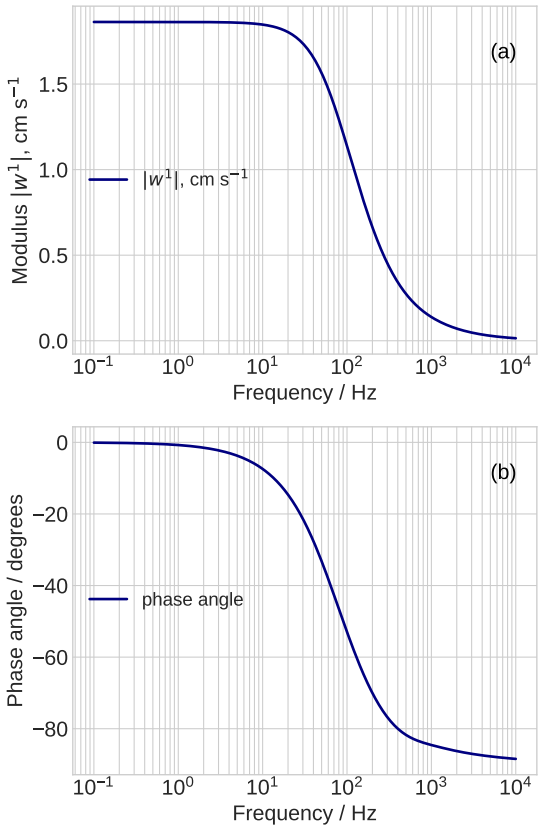

Figure 2: (a) The modulus and (b) the phase angle of velocity oscillations in the channel, Eq.(9).

frequency f_*, Eq.(10), the viscous friction induces a phase shift and the imaginary component of velocity grows. Above f_*, the phase angle between pressure and velocity further increases (Figure 2); in addition, the viscous forces damp the oscillations amplitude, and both the real and imaginary parts of $\langle \tilde{w}^1 \rangle$ decay (Figure 2).

In the limit of $\tilde{\omega} \to 0$, Eq.(9) in the dimension form reduces to the classic result

$$\lim_{\omega \to 0} \langle w^1 \rangle = \frac{R_h^2}{6\rho\nu} \left| \frac{\partial p^1}{\partial z} \right| \qquad (11)$$

Eq.(11) gives the contribution to steady–state flow velocity due to the static pressure gradient $\partial p^1/\partial z$ (Ref. [11]). Eq.(11) gives also the estimate for FVO maximal amplitude, which is achieved in the low frequency region (below 10 Hz in Figure 2a). Note that this amplitude is proportional to the channel cross section area and to the pressure gradient.

The amplitude p^1 is usually selected to keep the cell potential perturbations small for the sake of linearity, but sufficiently large to neglect the electric noise. However, the effect of p^1 on FVO amplitude is usually behind the scene. For example, in experiments [7], the channel cross–

Channel depth h and width, m	$0.1 \cdot 10^{-2}$
Channel length L, m	1.0
Inlet pressure p^{in}, Pa	10^5
Pressure perturbation amplitude p^1, Pa	10
Cell temperature T, K	273 + 65
Air density, ρ, kg m^{-3}	1.06
Air kinematic viscosity, ν, m^2 s^{-1}	$1.886 \cdot 10^{-5}$
Cell current density J, A m^{-2}	$0.1 \cdot 10^4$
Air flow stoichiometry λ,	2.0
Cell current density J, A m^{-2}	10^3
Tafel slope b, V	0.03
Double layer capacitance C_{dl}, F cm^{-3}	20
Exchange current density i_*, A m^{-3}	10^3
Oxygen diffusion coefficient in the CCL [12], D_{ox}, m^2 s^{-1}	$2 \cdot 10^{-8}$
Oxygen diffusion coefficient in the GDL [12], D_b, m^2 s^{-1}	$2 \cdot 10^{-6}$
Catalyst layer thickness l_t, m	$10 \cdot 10^{-6}$
Gas diffusion layer thickness l_b, m	$250 \cdot 10^{-6}$

Table 1: The cell parameters used in calculations. This is a typical set of parameters for laboratory PEMFC.

section area was $A = 3.08 \cdot 10^{-7}$ m^2 and the channel length 0.304 m. The pressure perturbation amplitude applied to this channel was 100 Pa. Taking for the estimate $\pi R_h^2 = A$, from Eq.(11) we get quite a significant low–frequency velocity oscillations amplitude about 0.24 m s^{-1}.

The effect of FVO on EPIS spectra of PEMFCs can be demonstrated using a plug–flow oxygen mass transport equation in channel:

$$\frac{\partial c_h}{\partial t} + \left(\langle w^0 \rangle + \langle w^1 \rangle\right) \frac{\partial c_h}{\partial z} = - \left. \frac{D_b}{h} \frac{\partial c_b}{\partial x} \right|_{x=l_t+l_b} \tag{12}$$

where c_h is the oxygen concentration in channel, D_b is the oxygen diffusion coefficient in the GDL of a thickness l_b, l_t is the CCL thickness, h is the channel depth. The right side of Eq.(12) describes oxygen "sink" from the channel flow through the channel/GDL interface. Substituting $c_h = c_h^0 + c_h^1, \quad c_h^1 \ll c_h^0$ into Eq.(12), subtracting the static equation for $\tilde{c}_h^0$ and neglecting the term $w^1 \partial c_h^1 / \partial z$, we get an equation for the small oscillating component c_h^1

$$\frac{\partial c_h^1}{\partial t} + \langle w^0 \rangle \frac{\partial c_h^1}{\partial z} + \langle w^1 \rangle \frac{\partial c_h^0}{\partial z} = - \left. \frac{D_b}{h} \frac{\partial c_b^1}{\partial x} \right|_{x=l_t+l_b} \tag{13}$$

With the dimensionless variables Eq.(2), Eq.(13) takes the form

$$\chi^2 \frac{\partial \tilde{c}_h^1}{\partial \tilde{t}} + \lambda \tilde{J} \frac{\partial \tilde{c}_h^1}{\partial \tilde{z}} + \lambda \tilde{J} \langle \tilde{w}^1 \rangle \frac{\partial \tilde{c}_h^0}{\partial \tilde{z}} = - \tilde{D}_b \left. \frac{\partial \tilde{c}_b^1}{\partial \tilde{x}} \right|_{\tilde{x}=1+\tilde{l}_b} \tag{14}$$

where

$$\lambda = \frac{4 F c_h^{in} h \langle w^0 \rangle}{L J} \tag{15}$$

is the air flow stoichiometry,

$$\chi = \sqrt{\frac{4 F c_h^{in} h l_t \nu}{\sigma_p b R_h^2}} = \sqrt{\frac{4 \pi F c_h^{in} l_t \nu}{\sigma_p b h}} \tag{16}$$

and the dimensionless mean current density and GDL oxygen diffusivity are given by

$$\tilde{j} = \frac{J l_t}{\sigma_p b}, \quad \tilde{D}_b = \frac{4 F D_b c_h^{in}}{\sigma_p b} \tag{17}$$

Note that in Eq.(16) circular channel cross–section area is replaced by the square channel area using $\pi R_h^2 = h^2$.

Substituting Fourier–transforms

$$\begin{aligned} \tilde{c}_h^1(\tilde{t}, \tilde{z}) &= \tilde{c}_h^1(\tilde{\omega}, \tilde{z}) \exp(\mathrm{i}\tilde{\omega}\tilde{t}), \\ \tilde{c}_b^1(\tilde{t}, \tilde{x}) &= \tilde{c}_b^1(\tilde{\omega}, \tilde{x}) \exp(\mathrm{i}\tilde{\omega}\tilde{t}), \\ \langle \tilde{w}^1(\tilde{t}) \rangle &= \langle \tilde{w}^1(\tilde{\omega}) \rangle \exp(\mathrm{i}\tilde{\omega}\tilde{t}) \end{aligned} \tag{18}$$

into Eq.(14) and taking into account that $\lambda \tilde{J} \partial \tilde{c}_h^0 / \partial \tilde{z} = -\tilde{j}_0(\tilde{z}) = -f_\lambda \tilde{J} (1 - 1/\lambda)^{\tilde{z}}$ (Ref. [13]) we finally get equation for the small perturbation amplitude $\tilde{c}_h^1$ in the $\tilde{\omega}$–space

$$\begin{aligned} \lambda \tilde{J} \frac{\partial \tilde{c}_h^1}{\partial \tilde{z}} = -\mathrm{i}\tilde{\omega} \chi^2 \tilde{c}_h^1 + f_\lambda \tilde{J} \langle \tilde{w}^1 \rangle \left(1 - \frac{1}{\lambda}\right)^{\tilde{z}} \\ - \tilde{D}_b \left. \frac{\partial \tilde{c}_b^1}{\partial \tilde{x}} \right|_{\tilde{x}=1+\tilde{l}_b}, \quad \tilde{c}_h^1(0) = \tilde{p}^1 \end{aligned} \tag{19}$$

where

$$f_\lambda = -\lambda \ln \left(1 - \frac{1}{\lambda}\right), \tag{20}$$

and $\langle \tilde{w}^1 \rangle$ is given by Eq.(9). Eq.(19) describes transport of the inlet oxygen perturbation along the channel taking into account FVO and oxygen "sink" to the GDL. Through–plane oxygen and proton transport equations leading to the formula for the term $\left. \tilde{D}_b \partial \tilde{c}_b^1 / \partial \tilde{x} \right|_{\tilde{x}=1+\tilde{l}_b}$ in Eq.(19) are described in [14]; the details of ζ calculation will be published elsewhere.

The concentration/pressure impedance calculated using Eq.(19), the model [14], and the parameters in Table 1 is shown in Figure 3. The contribution of term with the FVO $\langle \tilde{w}^1 \rangle$ is dominating: without this term, the spectrum diameter "shrinks" by an order of magnitude (Figure 4) and the high–frequency part of the spectrum changes strongly (cf. Figures 3 and 4). The main effect of pressure perturbation on the oxygen concentration in the cell is, thus, indirect, due to variation of air flow velocity in the cathode channel. Physically, oscillations of flow velocity in the channel are equivalent to oscillations of air stoichiometry. At low *static* stoichiometry, harmonic perturbation of this parameter strongly affect the spectra already at very low (10 Pa) amplitude of pressure perturbation due to effective perturbation of λ.

With the growth of λ, the Nyquist spectrum diameter strongly reduces (Figure 3). This effect has been reported in experiments of Engebretsen et al. [2] and Zhang et al. [8]. The effect of velocity oscillations on the EPIS spectra is thus maximal at low air flow stoichiometries.

Further, strong effect of FVO means that the flow field geometry determines the shape of EPIS spectra. In other words, EPIS spectra are best suited for studying the resistivity of oxygen transport in the flow field. At low stoichiometry, the EPIS spectra are only weakly sensitive to the oxygen transport in porous layers. For example, doubling of the GDL oxygen diffusivity practically does not change the spectra in Figure 3.

Experimental EPIS spectrum reported in Schiffer et al. [7] is shown in Figure 5. The model above does not take into account transients caused by the liquid water transport in the porous layers, and fitting the model to experimental spectra makes no sense. At this stage we can only note the similarity of model and experimental spectra.

Air supplied to the fuel cell cathode is usually humidified by passing through the humidifier. The presence of humidifier volume induces the phase shift between the pressure applied at the channel inlet and the inlet pressure [7]. The phase shift does not reduce the effect of FVO discussed above, but it makes interpretation of EPIS spectra even more complicated.

Finally we note that the phase shift of velocity oscillations varies in the range of 0.1 Hz to 10^3 Hz, as Figure 2b shows. Thus, below 0.1 Hz the effect of velocity oscillation on the spectra reduces to mere perturbation of the

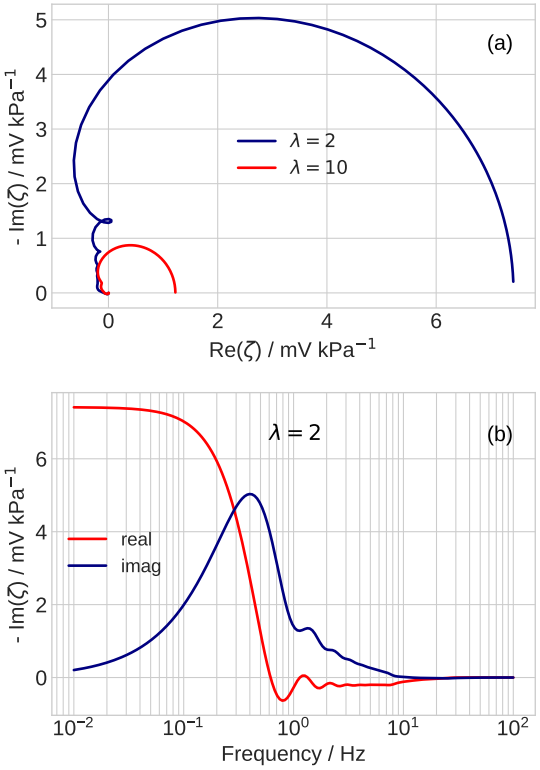

Figure 3: (a) The Nyquist spectrum of pressure impedance calculated using the model [14] and Eq.(19). (b) The frequency dependence of real and imaginary part of the spectrum in (a).

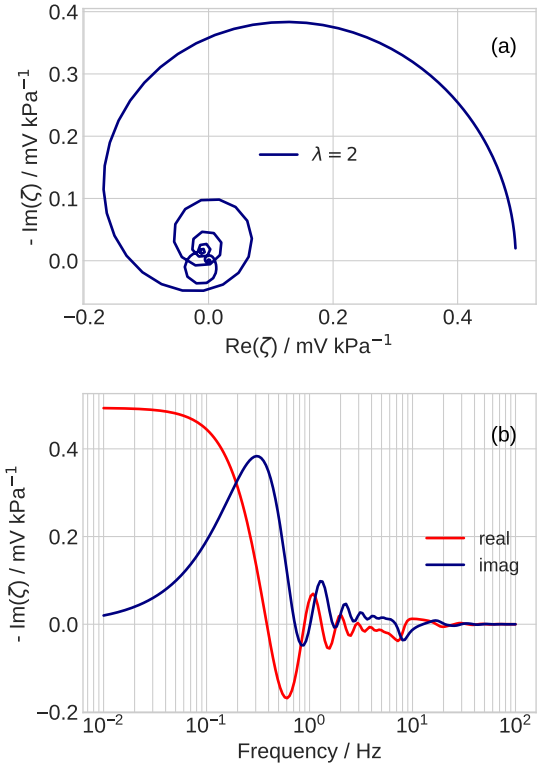

Figure 4: (a) The Nyquist spectrum of pressure impedance calculated using the model [14] and Eq.(19) *with zero FVO*, $\langle \tilde{w}^1 \rangle = 0$. (b) The frequency dependence of real and imaginary part of the spectrum in (a).

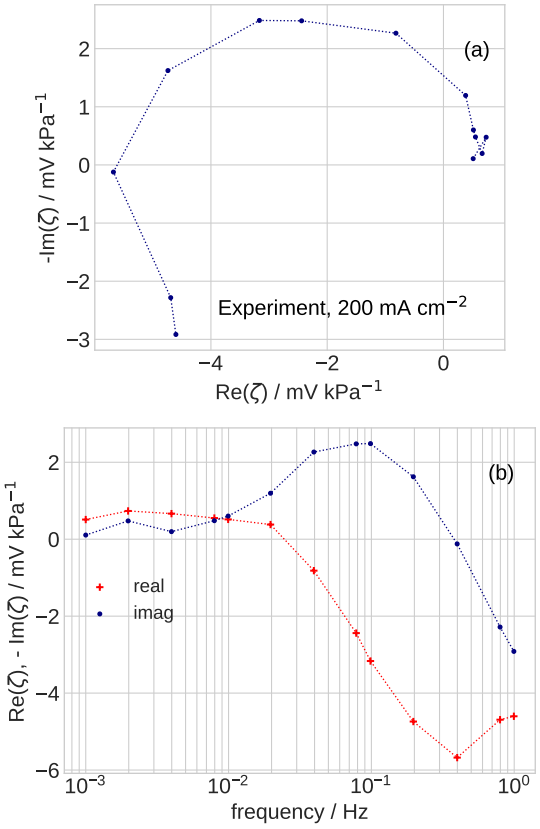

Figure 5: (a) The Nyquist spectrum of pressure impedance reported in [7]. The data are digitized from Figure 5 of [7]. (b) The frequency dependence of real and imaginary part of the spectrum in (a).

air flow stoichiometry. However, above 0.1 Hz the FVO changes the phase of oxygen concentration perturbation transported in the channel and it affects the EPIS spectrum in a more complicated way. Comparison of the spectra in Figures 3b and 4b shows that the peaks of $-\mathrm{Im}\,(\zeta)$ and the valleys of $\mathrm{Re}\,(\zeta)$ are located at different frequencies. This is due to the phase shift induced by FVO.

4. Conclusions

Analytical solution of a problem for the flow with oscillating velocity in a circular channel [10] is used to rationalize the effect of velocity oscillations on pressure impedance spectra of a PEMFC. Simple formulas for the average over channel radius axial flow velocity induced by the oscillating pressure gradient and for its static limit are derived. The characteristic frequency of the FVO is proportional to the air kinematic viscosity and inversely proportional to the channel cross section area. Numerical calculations show that at low air stoichiometries, the contribution of FVO to the cell pressure impedance dominates. This means that the main effect of pressure perturbations on the oxygen concentration is indirect, due to the flow velocity oscillations.

References

[1] A. M. Niroumand, W. Merida, M. Eikerling, M. Saif, Pressure–voltage oscillations as a diagnostic tool for PEFC cathodes, Electrochem. Comm. 12 (2010) 122–124. doi:10.1016/j.elecom.2009.11.003.

[2] E. Engebretsen, T. J. Mason, P. R. Shearing, G. Hinds, D. J. L. Brett, Electrochemical pressure impedance spectroscopy applied to the study of polymer electrolyte fuel cells, Electrochem. Comm. 75 (2017) 60–63. doi:10.1016/j.elecom.2016.12.014.

[3] A. Sorrentino, T. Vidakovic-Koch, R. Hanke-Rauschenbach, K. Sundmacher, Concentration–alternating frequency response: A new method for studying polymer electrolyte membrane fuel cell dynamics, Electrochim. Acta 243 (2017) 53–64. doi:10.1016/j.electacta.2017.04.150.

[4] A. Sorrentino, T. Vidakovic-Koch, K. Sundmacher, Studying mass transport dynamics in polymer electrolyte membrane fuel cells using concentration–alternating frequency response analysis, J. Power Sources 412 (2019) 331–335. doi:10.1016/j.jpowsour.2018.11.065.

[5] A. Sorrentino, K. Sundmacher, T. Vidakovic-Koch, Polymer electrolyte fuel cell degradation mechanisms and their diagnosis by frequency response analysis methods: A review, Energies 13 (2020) 5825. doi:10.3390/en13215825.

[6] A. V. Shirsath, S. Rael, C. Bonnet, L. Schiffer, W. Bessler, F. Lapicque, Electrochemical pressure impedance spectroscopy for investigation of mass transfer in polymer electrolyte membrane fuel cells, Current Opinion in Electrochem. 20 (2020) 82–87. doi:10.1016/j.coelec.2020.04.017.

[7] L. Schiffer, A. V. Shirsath, S. Raël, F. Lapicque, W. G. Bessler, Electrochemical pressure impedance spectroscopy for polymer electrolyte membrane fuel cells: A combined modeling and experimental analysis, J. Electrochem. Soc. 169 (2021) 034503. doi:10.1149/1945-7111/ac55cd.

[8] Q. Zhang, H. Homayouni, B. D. Gates, M. Eikerling, A. M. Niroumand, Electrochemical pressure impedance spectroscopy for polymer electrolyte fuel cells via back-pressure control, J. Electrochem. Soc. 169 (2022) 044510. doi:10.1149/1945-7111/ac6326.

[9] A. V. Shirsath, S. Raël, C. Bonnet, F. Lapicque, Electrochemical pressure impedance spectroscopy applied to polymer electrolyte membrane fuel cells for investigation of transport phenomena, Electrochim. Acta 363 (2020) 137157. doi:10.1016/j.electacta.2020.137157.

[10] T. Sexl, Über den von E. G. Richardson entdeckten Annulareffekt, Z. Phys. 61 (1930) 349–362. doi:10.1007/BF01340631.

[11] L. Landau, E. Lifshitz, Fluid Mechanics, Pergamon Press, NY, 1987.

[12] T. Reshetenko, A. Kulikovsky, Variation of PEM fuel cell physical parameters with current: Impedance spectroscopy study, J. Electrochem. Soc. 163 (9) (2016) F1100–F1106. doi:10.1149/2.0981609jes.

[13] A. A. Kulikovsky, The effect of stoichiometric ratio λ on the performance of a polymer electrolyte fuel cell, Electrochim. Acta 49 (4) (2004) 617–625. doi:10.1016/j.electacta.2003.09.016.

[14] A. Kulikovsky, Analytical impedance of PEM fuel cell cathode including oxygen transport in the channel, gas diffusion and catalyst layers, J. Electrochem. Soc. 169 (2022) 034527. doi:10.1149/1945-7111/ac5d97.

Nomenclature

$\tilde{}$	Marks dimensionless variables
c_b	Oxygen molar concentration in the GDL, mol m^{-3}
c_h	Oxygen concentration in the channel, mol m^{-3}
c_h^{in}	Reference (inlet) oxygen concentration, mol m^{-3}
D_b	Oxygen diffusion coefficient in the GDL, m^2 s^{-1}
F	Faraday constant, C mol^{-1}
i	Imaginary unit
J	Mean cell current density, A m^{-2}
h	Square channel depth, m
L	Channel length, m
l_t	CCL thickness, m
l_b	GDL thickness, m
p	Pressure, Pa
R_h	Circular channel radius, m
r	Radial coordinate, cm
T	Cell temperature, K
t	Time, s
w	Axial flow velocity in the channel, m s^{-1}
$\langle w \rangle$	Average over the channel radius flow velocity, m s^{-1}
x	Coordinate through the cell, m
z	Axial coordinate along the channel, m

Subscripts:

b	GDL
h	Channel

Superscripts:

0	Steady–state value
1	Small–amplitude perturbation

Greek:

ζ	Concentration impedance, V m^3 mol^{-1}
λ	Air flow stoichiometry
ν	Air kinematic viscosity, m^2 s^{-1}
ρ	Air density, kg m^{-3}
σ_p	CCL proton conductivity, S m^{-1}
ϕ	Dimensionless parameter, Eq.(4)
χ	Auxiliary dimensionless parameter, Eq.(16)
ω	Angular frequency of the AC signal, s^{-1}

Figure captions

1. (a) The Nyquist spectrum of velocity pulsations in the channel, Eq.(9). (b) The frequency dependence of real and imaginary part of Eq.(9). Parameters for the calculation are listed in the upper part of Table 1.
2. (a) The modulus and (b) the phase angle of velocity oscillations in the channel, Eq.(9).
3. (a) The Nyquist spectrum of pressure impedance calculated using the model [14] and Eq.(19). (b) The frequency dependence of real and imaginary part of the spectrum in (a).
4. (a) The Nyquist spectrum of pressure impedance calculated using the model [14] and Eq.(19) *with zero FVO,* $\langle \tilde{w}^1 \rangle = 0$. (b) The frequency dependence of real and imaginary part of the spectrum in (a).
5. (a) The Nyquist spectrum of pressure impedance reported in [7]. The data are digitized from Figure 5 of [7]. (b) The frequency dependence of real and imaginary part of the spectrum in (a).